Arctic September Sea Ice Concentration Biases in CMIP6 Models and Their Relationships with Other Model Variables

CLAUDE FRANKIGNOUL,[a,b] LEA RAILLARD,[c] BRADY FERSTER,[a,d] AND YOUNG-OH KWON[b]

[a] *UMR LOCEAN, Sorbonne Université, IRD, MNHM, CNRS, IPSL, Paris, France*
[b] *Woods Hole Oceanographic Institution, Woods Hole, Massachusetts*
[c] *Laboratoire de Météorologie Dynamique, IPSL, Paris, France*
[d] *Department of Earth and Planetary Sciences, Yale University, New Haven, Connecticut*

(Manuscript received 27 July 2023, in final form 18 April 2024, accepted 2 May 2024)

ABSTRACT: The models that participated in the Coupled Model Intercomparison Project (CMIP) exhibit large biases in Arctic sea ice climatology that seem related to biases in seasonal atmospheric and oceanic circulations. Using historical runs of 34 CMIP6 models from 1979 to 2014, we investigate the links between the climatological sea ice concentration (SIC) biases in September and atmospheric and oceanic model climatologies. The main intermodel spread of September SIC is well described by two leading EOFs, which together explain ~65% of its variance. The first EOF represents an underestimation or overestimation of SIC in the whole Arctic, while the second EOF describes opposite SIC biases in the Atlantic and Pacific sectors. Regression analysis indicates that the two SIC modes are closely related to departures from the multimodel mean of Arctic surface heat fluxes during summer, primarily shortwave and longwave radiation, with incoming Atlantic Water playing a role in the Atlantic sector. Local and global links with summer cloud cover, low-level humidity, upper or lower troposphere temperature/circulation, and oceanic variables are also found. As illustrated for three climate models, the local relationships with the SIC biases are mostly similar in the Arctic across the models but show varying degrees of Atlantic inflow influence. On a global scale, a strong influence of the summer atmospheric circulation on September SIC is suggested for one of the three models, while the atmospheric influence is primarily via thermodynamics in the other two. Clear links to the North Atlantic oceanic circulation are seen in one of the models.

KEYWORDS: Arctic; Sea ice; Climate models

1. Introduction

Since the 1980s, the warming of high northern latitudes has been at least 2–3 times faster than the global average rate, a phenomenon known as Arctic amplification (e.g., Serreze et al. 2009; Huang et al. 2017). This warming is associated with a decline and a thinning of Arctic sea ice (e.g., Screen et al. 2018; Previdi et al. 2021), and it is mostly attributed to anthropogenic forcing. In addition, internal variability has also played a role, but its exact contribution to sea ice change remains debated (e.g., England et al. 2019; Ding et al. 2019). Climate model projections suggest that the whole Arctic Ocean may become ice-free in September by the middle of this century (Notz and Sea-Ice Model Intercomparison Project Community 2020). However, the exact timing varies between models, in part because the models that participated in the Coupled Model Intercomparison Project (CMIP) phase contain large biases in the simulated sea ice climatology and its decreasing trend (e.g., Topal et al. 2020; Long et al. 2021). Confidence in the model projections depends on these biases, hence on the model's ability to reproduce the main features of the present-day climate and its observed evolution. Sea ice biases are generally considered to be affected by the model resolution and configuration of the sea ice component model. However, Long et al. (2021) evaluated the ability of 35 CMIP6 models to simulate Arctic sea ice climatology by comparing simulated results with observation and found no dependence on model resolution in late summer. In addition, no dependence of September sea ice concentration (SIC) on the sea ice component model could be seen in this study. Since SIC discrepancies between observation and models are the largest in September, the September SIC biases may be largely due to model representation of the atmospheric and oceanic circulations although sea ice thickness at the end of the growth season may also contribute. This would be consistent with observational and modeling evidence that atmospheric variability substantially contributes to the variability and decline of the Arctic sea ice in September (e.g., Kay et al. 2011; Wettstein and Deser 2014; Jahn et al. 2016; Ding et al. 2017, 2019; Baxter et al. 2019; Topal et al. 2020).

It is thus of interest to investigate the links between the Arctic sea ice biases in September when SIC is at its seasonal minimum and other atmospheric and oceanic biases in climate models. Here, we focus on the links between representations of September SIC climatology and that of the climatology of other model variables. We base the climatological means on the 1979–2014 period when sea ice was well observed by satellite imagery, and natural and anthropogenic forcings derived from observations are prescribed in the historical simulations by CMIP6 models. Focusing on a 36-yr climatology and, when

Supplemental information related to this paper is available at the Journals Online website: https://doi.org/10.1175/JCLI-D-23-0452.s1.

Corresponding author: Claude Frankignoul, claude.frankignoul@locean.ipsl.fr

DOI: 10.1175/JCLI-D-23-0452.1

possible, averaging over ensemble members would strongly reduce the uncertainty due to internal variability that affects the evolution of September SIC and other variables. In this paper, we investigate the links between the intermodel spread of September SIC climatology and that of atmospheric and oceanic climatologies, which are considered primarily during summer to account for the limited sea ice persistence (Blanchard-Wrigglesworth et al. 2011) and response time. We will show that the multimodel mean (MMM) September SIC climatology is biased relative to observations although internal variability may contribute to the latter. The biases of MMMs cannot be investigated by the methodology used in this paper, but they should not substantially affect the links between the intermodel spreads of the departures from MMM climatology.

We first establish the main modes of the intermodel spread of the climatological September SIC, which represents the main departures from the MMM climatology. Using regression analysis, we then investigate their relationships with the departures from the MMM of other atmospheric and oceanic climatologies. The analysis does not consider relations between MMMs nor depends on the existence of a trustable observational basis. Moreover, it will be shown that the departures from the MMM are usually broadly similar to actual biases (against the observation) so that our analysis informs the relationships between biases in climate models. Mohino et al. (2019) used a similar strategy in a different context. Although correlations do not imply causality, we may tentatively interpret them in this way when they reflect a plausible physical mechanism. For each CMIP6 model, the atmospheric and oceanic departures from the MMM can also be compared to those reconstructed from main SIC modes, thus providing useful information on their potential impact on September SIC. It will be shown that such comparison largely varies between models on the global scale.

Section 2 describes the data, the 34 CMIP6 models, and the analysis method. In section 3, the September SIC biases and their two main modes of intermodel variations are documented. The links of these modes with atmospheric and oceanic variables are discussed in section 4, first over the Arctic, then north of 20°S. In section 5, the departures from the MMM and those reconstructed from their links to the two SIC modes are compared for three models chosen for illustration, i.e., IPSL-CM6-LR, CESM2, and Norwegian Climate Prediction Model, version 1 (NorCPM1), which have more than 10 ensemble members and are unlikely to be significantly affected by internal variability. The first two models were a priori chosen because they have been and still are extensively used by the authors. As it turned out that both models underestimate the mean September SIC, albeit differently, we added a model that strongly overestimates it and somewhat arbitrarily chose NorCPM1. Conclusions and discussion are given in section 6.

2. Data and methods

a. Data

Model data and observations are based on 1979–2014 means. The observed SIC in September is taken from the National Snow and Ice Data Center (NSIDC) on a polar stereographic grid at 25 km × 25 km resolution (NOAA/NSIDC climate data record of passive microwave sea ice concentration, version 4, Meier et al. 2021). The simulated September SIC climatology is computed for each of the 34 CMIP6 models listed in Table 1. Several atmospheric variables are considered, namely, 2-m air temperature [surface air temperature (SAT)]; temperature (T925) and specific humidity (Q925) at 925 hPa; the approximate inversion level over the Arctic; sea level pressure (SLP); zonal wind at 850 hPa (U850); geopotential height at various levels, in particular 250 hPa (Z250) and 30 hPa (Z30); total cloud cover (the cloud area fraction for the whole atmospheric column); surface heat fluxes (positive upward unless specified); and surface wind stress. Monthly mean atmospheric data were recovered for each model from the IPSL CMIP6 database (https://esgf-node.ipsl.upmc.fr/search/cmip6-ipsl/), and climatological summer averages (June–August) over the 1979–2014 period were calculated. When ensemble simulations are available, the average over all available members is used to reduce the role of internal variability. "Observed" climatological summer means are derived from the fifth major global reanalysis produced by the European Centre for Medium-Range Weather Forecasts (ECMWF) (ERA5) (Hersbach et al. 2020). Summer mean sea surface salinity (SSS), SIC, and March SIC are also calculated in each model. All data are interpolated on the same 1° × 1° rectilinear grid. For simplicity, these variables are only considered north of 20°S. The links with yearly mean Atlantic meridional overturning circulation (AMOC) are also investigated although the AMOC was only available in depth coordinate and 29 of the 34 models; it is considered at 35°, 40°, 45°, 50°, 55°, and 60°N. Climatological summer and yearly mean ocean heat transport (OHT) across the Barents Sea Opening in the 1979–2014 period were estimated from monthly data kindly provided by Shu et al. (2022) for 12 of the 34 CMIP6 models (asterisk in Table 1).

b. Methods

Regression analysis is used to establish the relationships between the intermodel spread of the September SIC climatology and the corresponding departures of other variables among the 34 CMIP6 models. For simplicity, we use summer means for the atmosphere, which gives equal weight to June, July, and August even though forcing in each month should contribute differently to September SIC, not only because of the seasonal cycle in SIC and thickness but also because September SIC may be more affected by atmospheric forcing in one particular month (e.g., Luo et al. 2023). In addition, summer means do not represent atmospheric forcing in previous seasons although, for example, cloudiness and the associated radiative forcing during spring may have more impact than during summer on sea ice properties in September (e.g., Kapsch et al. 2016; Cox et al. 2016).

The main modes of intermodel spread of the September SIC climatology are derived from an area-weighted EOF analysis of the mean September SIC (after removing MMM). Only the first two eigenvalues are well separated based on the rule of thumb of North et al. (1982), who estimated when the sampling errors become comparable to or larger than the

TABLE 1. Model name, institute name, number of available members (N), sea ice component model, and its longitudinal resolution (in number of zonal grids) for the 34 CMIP6 models. An asterisk next to the model name indicates that OHT was available. More details can be found at https://pcmdi.llnl.gov/CMIP6/.

Model name	Institute	N	Sea ice zonal resolution
TaiESM1	Academia Sinica, Taiwan	1	CICE4 (320)
BCC-CSM2-MR	Beijing Climate Center (BCC)	3	SIS 1.0 (360)
BCC-ESM1	BCC	3	SIS (360)
CAMS-CSM1-0	Chinese Academy of Sciences (CAS)	3	SIS 1.0 (320)
FGOALS-f3-L	CAS	3	CICE4.0 (360)
FGOALS-g3	CAS	6	CICE4.0 (360)
CanESM5*	Canadian Centre for Climate Modelling and Analysis (CCCma)	65	LIM2 (360)
CanESM5-CanOE*	CCCma	3	LIM2 (360)
CMCC-CM2-HR4	Centro Euro-Mediterraneo sui Cambiamenti Climatici	1	CICE4.0 (1442)
CNRM-CM6-1*	Centre National de Recherches Météorologiques-CERFACS	21	GELATO 6.1 (362)
CNRM-CM6-1-HR*	CNRM-CERFACS	1	GELATO 6.1 (1442)
CNRM-ESM2-1*	CNRM-CERFACS	27	GELATO 6.1 (362)
ACCESS-ESM1-5*	Commonwealth Scientific and Industrial Research Organisation (CSIRO)	40	CICE4.1 (360)
ACCESS-CM2*	CSIRO-Australian Research Council Centre of Excellence for Climate System Science (ARCCSS)	3	CICE4.1 (360)
E3SM-1-1	E3SM-PROJECT	1	MPAS-Sea Ice (720)
E3SM-1-1-ECA	E3SM-PROJECT	1	MPAS-SI (720)
EC-Earth3-AerChem	European Consortium	2	LIM3 (362)
EC-Earth3-Veg*	European Consortium	8	LIM 3 (362)
MPI-ESM1-2-HAM	HAMMOZ-Consortium	3	Unnamed (256)
INM-CM4-8	Institute for Numerical Mathematics (INM), Russia	1	INM-ICE1 (360)
INM-CM5-0	INM	10	INM-ICE1 (360)
IPSL-CM6A-LR*	L'Institut Pierre-Simon Laplace	33	LIM3 (362)
MIROC6	Japan Agency for Marine-Earth Science and Technology	50	COCO4.9 (360)
HadGEM3-GC31-LL*	Met Office Hadley Center	4	CICE-HadGEM3-GSI8 (360)
HadGEM3-GC31-MM	Met Office Hadley Center	4	CICE-HadGEM3-GSI8 (1440)
MPI-ESM1-2-HR	Max Planck Institute (MPI) for Meteorology	10	Unnamed (384)
MPI-ESM1-2-LR	MPI	10	Unnamed (256)
GISS-E2-1-G-CC	NASA Goddard Institute for Space Studies (GISS)	10	GISS SI (144)
GISS-E2-1-H	NASA GISS	25	GISS SI (144)
CESM2*	National Center for Atmospheric Research (NCAR)	11	CICE 5.1 (320)
CESM2-FV2	NCAR	3	CICE 5.1 (320)
CESM2-WACCM*	NCAR	3	CICE 5.1 (320)
CESM2-WACCM-FV2	NCAR	3	CICE 5.1 (320)
NorCPM1	Norwegian Climate Consortium	30	CICE4 (360)

spacing between neighboring eigenvalues, so that the EOFs are effectively degenerated and cannot be used as an approximation of the true eigenvectors. Hence, only the first two EOFs are considered, representing 65% of the intermodel variance. The first two principal components (PCs) indicate how each model contributes to the SIC EOFs. The departures from the MMM climatology of an atmospheric or oceanic variable Y are then regressed onto PC1 and PC2. This is written for each model $m = 1, 34$:

$$Y(x, m) - \overline{Y(x)} = a(x)\mathrm{PC1}(m) + b(x)\mathrm{PC2}(m) + r(x, m), \tag{1}$$

where $r(x, m)$ is a residual with zero mean whose norm is minimized. The overbar denotes MMM, and x is the spatial dimension. If an atmospheric or oceanic variable is not available from the database for a particular model, the regression maps a, b, and the MMM are calculated from the remaining models, but it is only a slightly limiting factor for the AMOC. Statistical significance in the a and b patterns is estimated at each grid point by Student's t test, assuming for simplicity independence between models, although it somewhat overestimates statistical significance since some models share the same components. Field significance is then estimated at both the 5% and 10% significance levels following Wilks (2016), using $\alpha_{\mathrm{FDR}} = 0.1$ and 0.2, respectively. In the Arctic domain, the false discovery rate (FDR) procedure is applied to the 65°–90°N domain but limited to grid points above sea ice and the ocean for variables that primarily characterize local air–sea ice interactions (SIC, SAT, T925, Q925, surface heat flux, cloudiness, SSS, and surface wind stress), while the whole 65°–90°N domain is considered for large-scale variables (SLP, U850, Z250, and Z30). In the global domain, the FDR procedure is applied to all grid points north of 20°S. Note that grid points deemed "FDR significant" in the polar domain may not be FDR-significant in the global domain. We also applied the FDR approach to the 20°–90°N domain which might

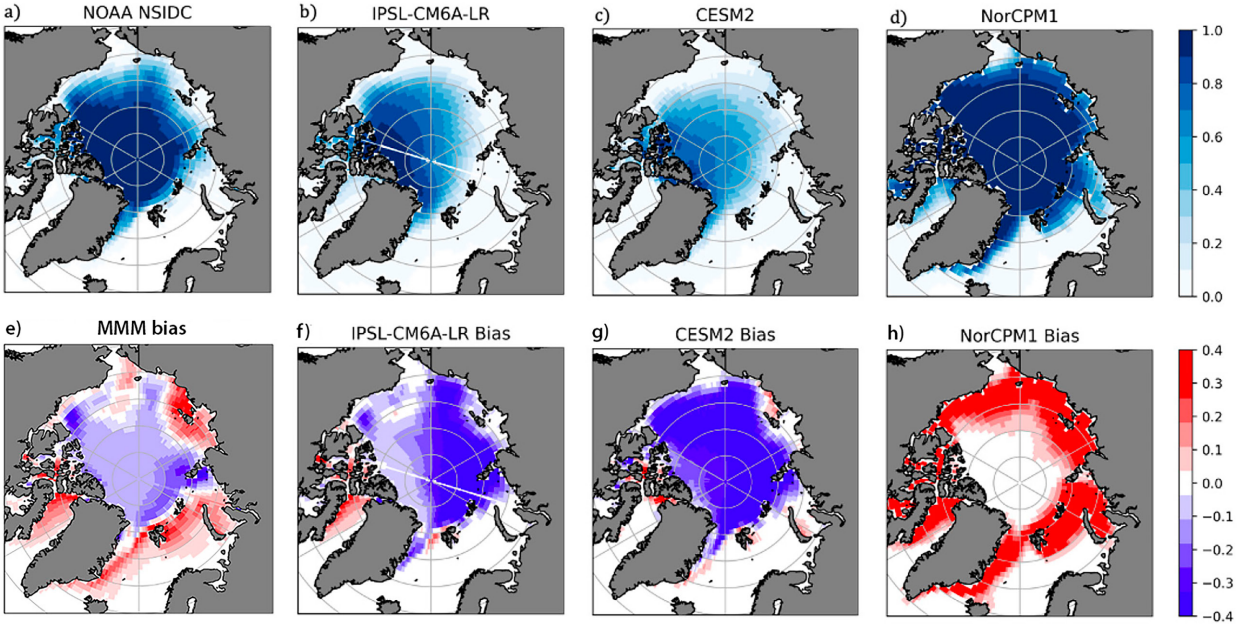

FIG. 1. (a) Observed and (b)–(d) simulated SIC September climatology (1979–2014) and (f)–(h) corresponding bias in three CMIP6 models. Also represented is (e) the MMM bias of the 34 CMIP6 models. The 34 model biases are shown in Fig. S1.

better represent extratropical atmospheric dynamics, but the results are nearly identical to those in 20°S–90°N and are not presented. To verify whether the analysis is significantly affected by internal variability, we also performed the analysis using the 14 models that had at least 8 ensemble members.

3. September sea ice concentration biases

Figure 1 shows the mean September SIC in the Arctic for the 1979–2014 period in the observations and in three climate models that we chose for illustration (top): IPSL-CM6-LR (Boucher et al. 2020), CESM2 (Danabasoglu et al. 2020), and NorCPM1 (Bethke et al. 2019), as well as their bias (bottom). Figure 1 in the online supplemental material shows for completeness the climatological mean September bias for each of the 34 CMIP6 models, suggesting that there is no obvious outlier. Consistent with Fig. 1, Boucher et al. (2020) and Danabasoglu et al. (2020) showed that IPSL-CM6A-LR and CESM2, respectively, mostly underestimate the mean SIC (negative bias). On the other hand, Shen et al. (2021) found that NorCPM1 strongly overestimates the mean SIC. The MMM (Fig. 1e) underestimates the SIC in the central Arctic, the Beaufort Sea, and near the Taymyr Peninsula but overestimates SIC in Baffin Bay, the Greenland and Barents Seas, and part of the Kara and Laptev Seas. The largest divergence between models is found in the East Greenland Current, off Svalbard, in the northern Barents–Kara Seas, and in the Beaufort Sea (not shown). As noted above, our analysis only informs the relationship between the departures from the MMM. However, for SIC, they largely resemble the original total biases, as illustrated for the three models (cf. Fig. 2, top with Figs. 1f–h).

The first two EOFs of the intermodel spread of the September SIC are shown in Fig. 3 (unweighted SICs are used for display). The PCs, which indicate how each model contributes to the SIC biases, are standardized and the EOFs scaled correspondingly so that the SIC amplitude is given by the EOFs. EOF1, which represents half of the variance, is a negative monopole (too small SIC) over the whole Arctic, with maximum amplitude in the East Greenland Sea, the Barents–Kara Seas, and the Laptev and East Siberian Seas. EOF2 has slightly smaller amplitude and is a dipole with less SIC in the Barents–Kara Seas and more SIC in the East Siberian, Chukchi and Beaufort Seas.

As shown by the PCs, the EOF1 pattern is strongly amplified (large positive PC1) in CNRM-CM6-1-HR, IPSL-CM6-LR, MPI-ESM1-2-HR and MPI-ESM1-2-LR, GISS-E2-1-G-CC, and CESM2, thus having underestimated SIC referenced to MMM. Similarly, negative values of PC1 reflect too large SIC, in particular in BCC-ESM1, FGOALS-g3, GISS-E2-1-H, and NorCPM1. Models such as CESM2 and NorCPM1 have PC1 and PC2 of opposite sign, which makes more evenly distributed sea ice biases through the domain, while models with PC1 and PC2 of the same sign, like the BCC models and FGOALS-g3, show more contrasted biases between the Atlantic and Pacific sectors. No PC dependence on the configuration of the sea ice component model (Table 1) could be detected in Fig. 3.

The departure from the MMM September SIC bias of one model (mth model) can be compared with its reconstruction S^* based on EOF1 and EOF2, defined by

$$S^*(x, m) = \mathrm{PC1}(m) \times \mathrm{EOF1}(x) + \mathrm{PC2}(m) \times \mathrm{EOF2}(x). \quad (2)$$

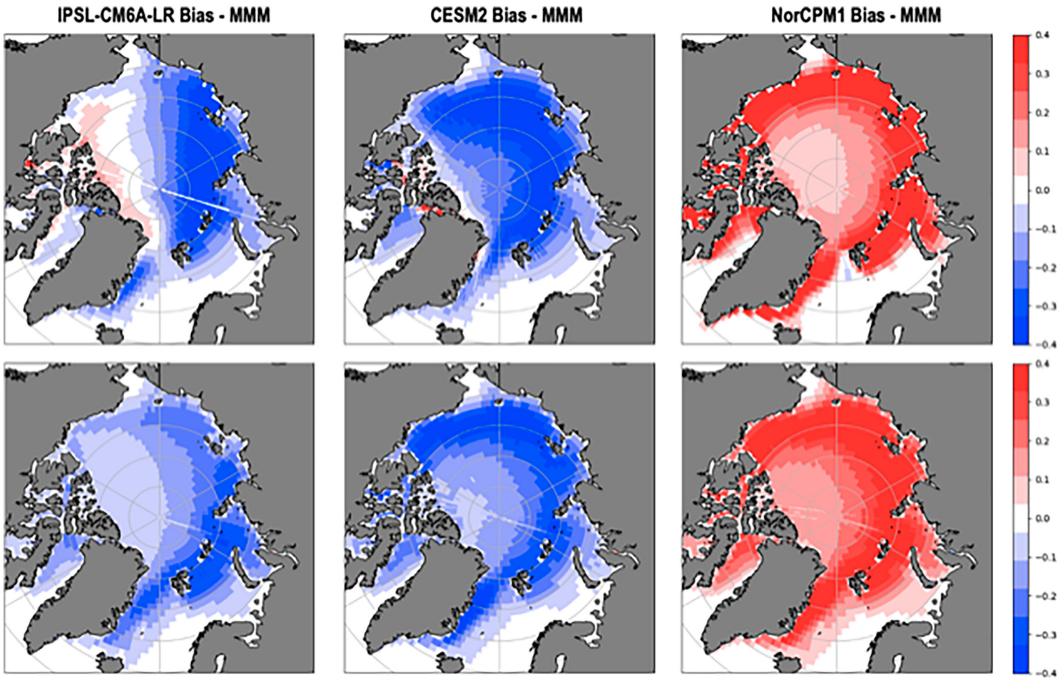

FIG. 2. (top) September SIC bias shown as the departure from the MMM and (bottom) its reconstructed SIC bias based on EOF1 and EOF2 for the three climate models.

As illustrated in Fig. 2, the reconstructed SIC biases (bottom) largely resemble the original model biases (top), but the amplitudes do not match, which is consistent with the limited number of retained EOFs.

To investigate the possible influence of internal variability, the analysis was redone using the models that had at least 8 members, thus with 14 models (Table 1). The first SIC EOF is little altered but represents more variance (63.1%), and PC1 is broadly similar to the values in the 34-model analysis albeit with some changes in amplitude but no change in sign (not shown). Based on North et al. (1982)'s rule of thumb, the first mode is well separated, but the second EOF (11.7% of the variance) is effectively degenerated, as the sampling error in the second eigenvalue is nearly equal to its separation from the third eigenvalue (7.2% of the variance). This primarily reflects the smaller sample and model diversity.

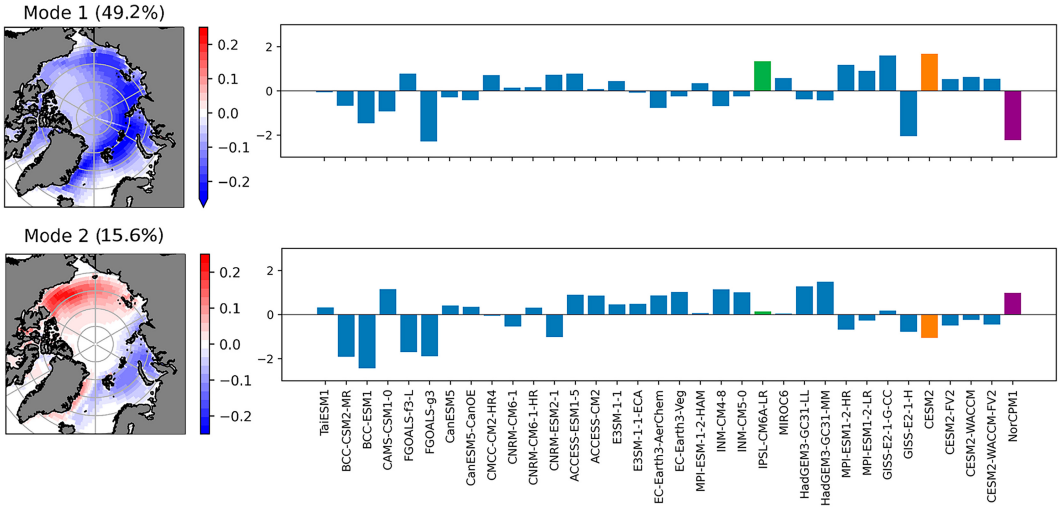

FIG. 3. September SIC intermodel EOF1 and EOF2 (unweighted for display) and associated PCs (model series). The portion of total intermodel variance explained by each mode is indicated with the EOF patterns. The green, red, and purple bars indicate the three models shown in Figs. 1 and 2.

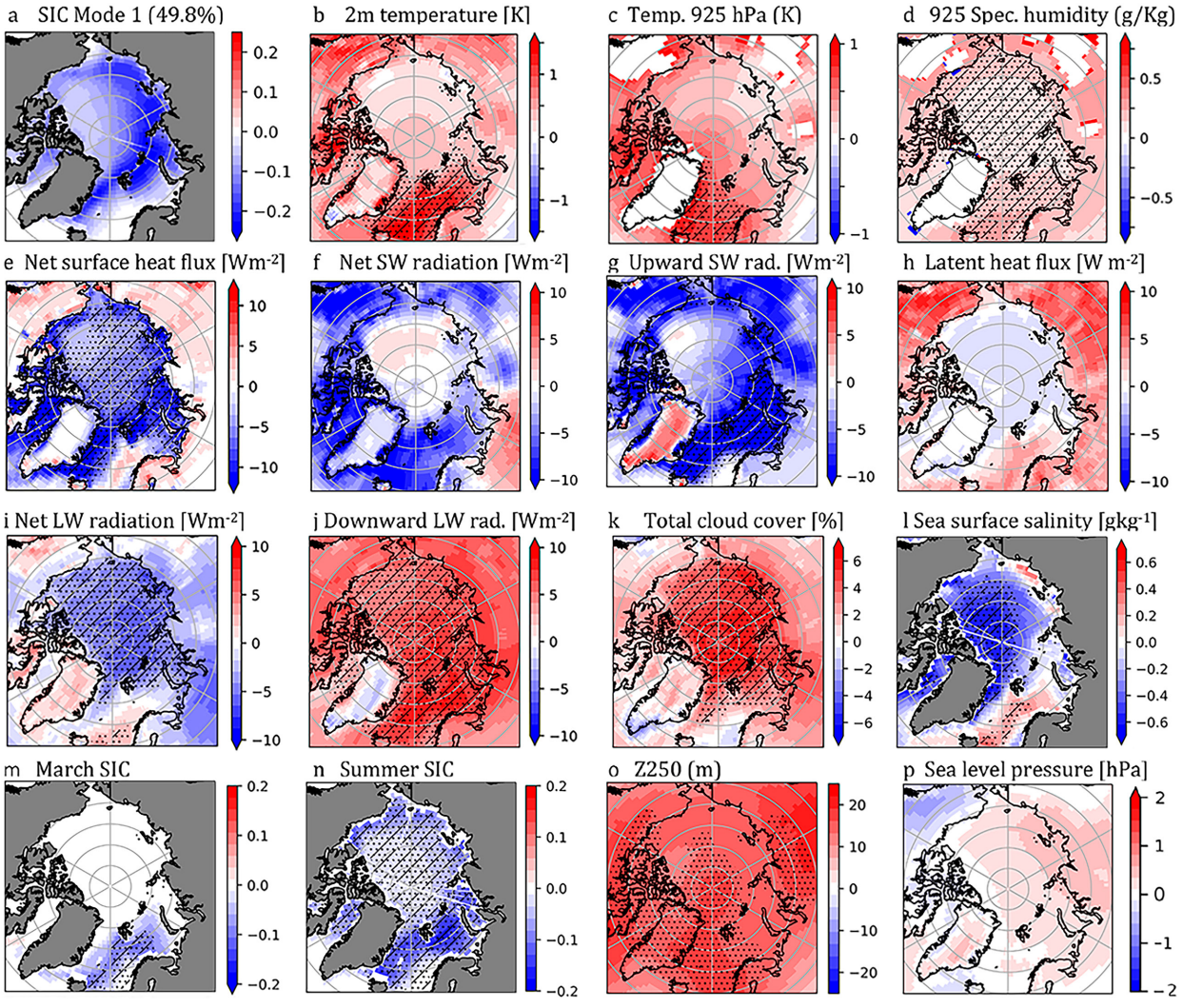

FIG. 4. (a) SIC EOF1 and (b)–(p) regression of various atmospheric and oceanic departures from the MMM (as indicated) on PC1 in the Arctic domain. All the heat fluxes are defined as positive upward, except the downward LW radiation, and departures are for summer (June–August) except in (m). Black dots (hatching) indicate elements that satisfy the FDR criterion north of 65°N (excluding continents; except for SLP and Z250) at the 10% (5%) significance level.

4. Links to the other model biases

a. Links with SIC mode 1

In the Arctic domain, the regression on PC1 shows that the September SIC mode 1 is linked to warmer summer SAT than the MMM (warmer SAT) in the whole Arctic domain (Fig. 4b), but the amplitude is very small except over the Nordic seas and the Barents Sea. As these regions are either ice-free or have a rather small SIC during summer (Fig. 4n), the significant links mostly occur where the air is largely in contact with the open ocean. That there is no significant correlation where summer SIC is large could also reflect that in the melting season, SAT generally varies little from 0°C. The links with T925 are broadly similar, but FDR-significant warming is mostly limited to the Nordic seas (Fig. 4c). Mode 1 has a highly significant positive link with Q925 over the whole Arctic Ocean, with largest amplitude over the Nordic seas (Fig. 4d). During summer, the low-level atmosphere associated with mode 1 is thus more humid and warmer in the North Atlantic sector, where the SIC is already biased low (Fig. 4n).

Unlike for SAT, there is a close spatial correspondence between the negative SIC of mode 1 and net negative surface heat flux (i.e., into sea ice or ocean) during summer (Fig. 4e), which should reinforce the low SIC in September. In the Greenland Sea, Baffin Bay, and much of the Barents Sea, the net surface shortwave (SW) radiation is negative albeit not FDR-significant (Fig. 4f). It is dominated by the underestimation of its upward component (FDR-significant in the North Atlantic sector; Fig. 4g), which is seemingly due to the underestimation of summer SIC and thus surface albedo, which limits the reflection of incoming SW radiation and sustains the September SIC bias by ice–albedo feedback. Over the ice-

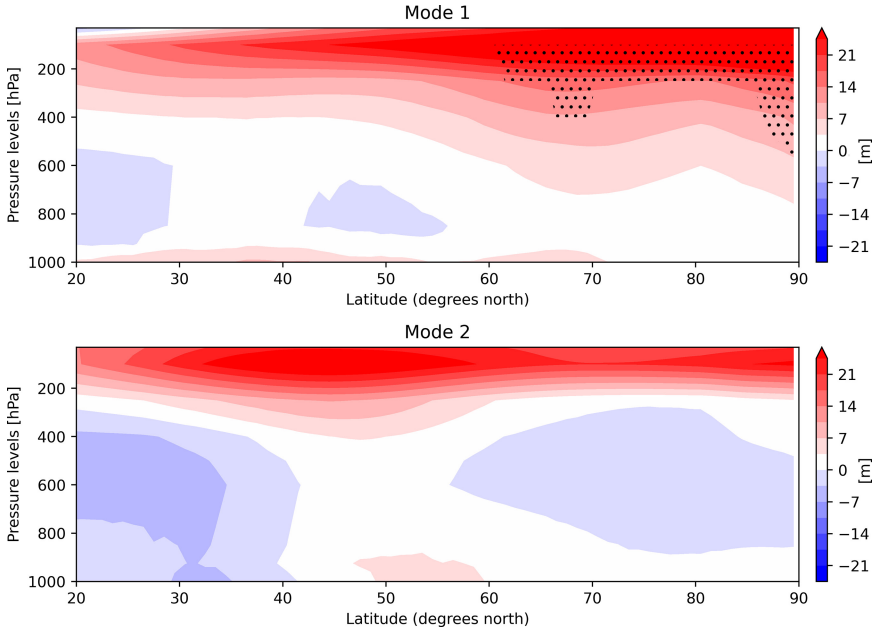

FIG. 5. Zonally averaged geopotential height departure from the MMM in summer (m) regressed on SIC (top) PC1 and (bottom) PC2, respectively. Black dots indicate the local statistical significance at the 10% level.

covered central Arctic and from the Laptev Sea to the Chukchi Sea, the net surface heat flux is dominated by negative longwave (LW) radiation (Fig. 4i). This LW radiation departure from the MMM is largely due to its downward component (Fig. 4j), consistent with larger total cloud cover over sea ice (Fig. 4k) and larger low-level specific humidity (Fig. 4d). There is no FDR-significant link with turbulent heat fluxes (e.g., Fig. 4h). Although summer LW radiation also contributes to the low SIC in the Atlantic sector, the SIC linked to mode 1 is also affected there by SW radiation, perhaps because open water is the norm for a longer period in summer in the Atlantic sector. We speculate that this reflects an oceanic influence.

Since SAT and sea surface temperature (SST) are usually so similar above open water that SAT can be used as a proxy for SST, the incoming Atlantic waters into the Arctic linked to mode 1 are warmer during summer than the MMM. Although it is not FDR-significant, the surface latent heat flux in the Norwegian and Barents Seas may correspondingly reflect larger ocean heat loss (Fig. 4h). Mode 1 is also associated with significant positive SSS in this region (Fig. 4l), consistent with warmer and saltier Atlantic inflow. This could be indicative of a stronger OHT into the Arctic, but it could not be verified because OHT was only available for 12 of the 34 CMIP6 models, and there was much scatter in their relationship with the SIC PCs. By contrast, SSS is negative in the broader central Arctic (Fig. 4l), consistent with the underestimated summer SIC and thus more melting (Fig. 4n). As Zhang (2015) and Årthun et al. (2019) showed

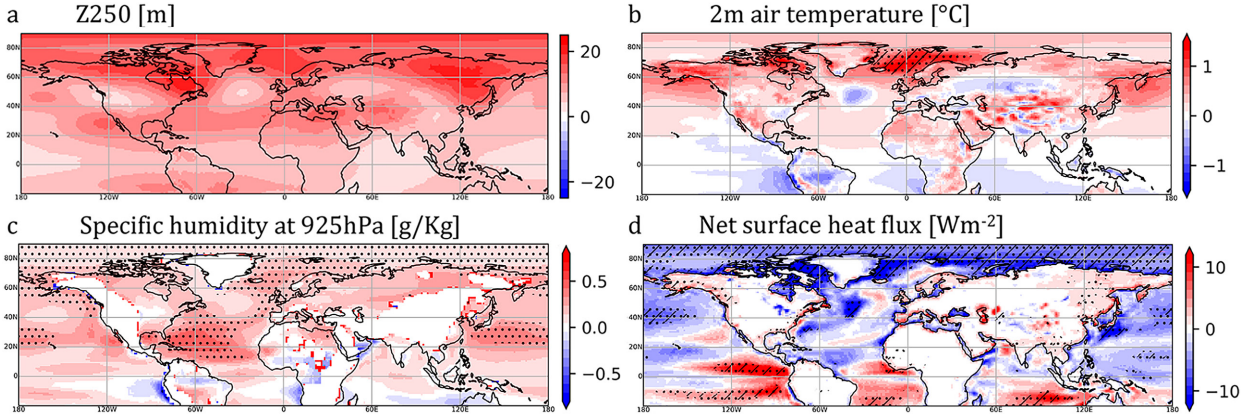

FIG. 6. (a)–(d) Regression of several atmospheric variables (as indicated) during summer on SIC PC1, north of 20°S. The heat fluxes are positive upward. Black dots (hatching) indicate elements that satisfy the FDR criterion north of 20°S at the 10% (5%) significance level.

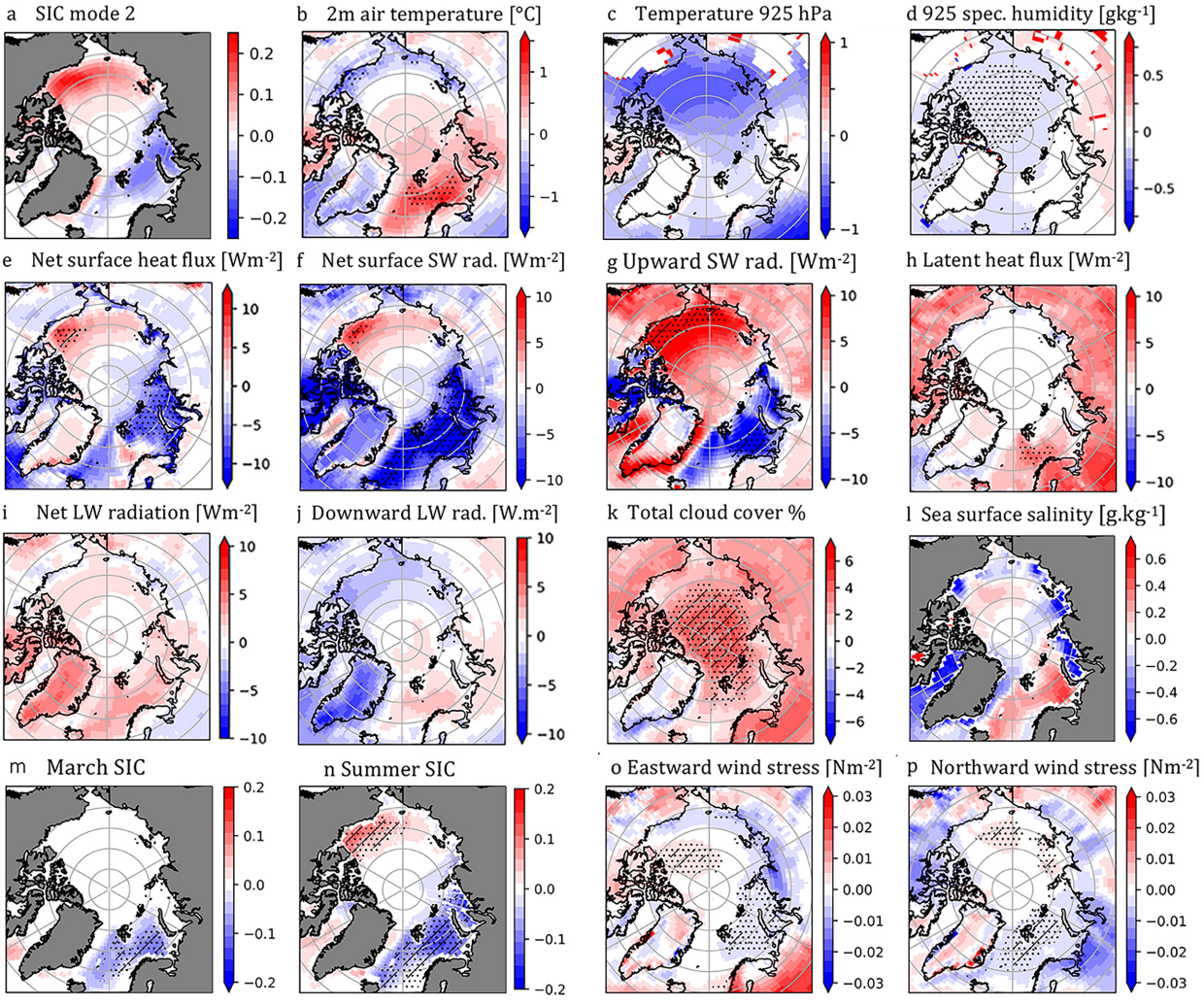

FIG. 7. (a) September SIC EOF2 and (b)–(p) regression of various atmospheric and oceanic departures from the MMM (as indicated) on PC2 in the Arctic domain. All the heat fluxes are defined as positive upward, except for the downward LW radiation, and departures are for summer except in (m). Black dots (hatching) indicate elements that satisfy the FDR criterion north of 65°N (excluding continents; except for SLP and Z250) at the 10% (5%) significance level.

that OHT is a critical driver and good predictor of winter SIC in the Barents Sea, a larger OHT would also be consistent with the large negative SIC seen there in March (Fig. 4m) so that SIC is biased low in the Barents Sea throughout the year. Local atmospheric dynamics has little influence on mode 1 since PC1 has no significant links with Arctic surface wind stress (not shown).

Interestingly, mode 1 is associated with an elevated upper troposphere over the whole Arctic domain, as seen at 250 hPa (Fig. 4o). The anticyclonic circulation is largest above Greenland, northeastern Canada, and the Nordic seas, albeit only 10% significant. Since a stronger upper-level anticyclone induces downward motion, adiabatic warming, and increased low-level cloudiness and relative humidity over the Arctic (e.g., Huang et al. 2021), this suggests that high-latitude tropospheric circulation during summer contributes to the negative SIC bias of SIC September mode 1. There is no significant signal in SLP (Fig. 4p) and at 30 hPa.

The regressions were also estimated for the 14 models that had at least 8 ensemble members. The patterns were similar, but FDR significance was often lower, in particular for sea surface salinity and March SIC, as expected from the smaller sample size. However, the positive regression of SLP was larger than in Fig. 4p and 10% FDR-significant over much of the Arctic (not shown). Noteworthy is that the link with Z250 remained 10% FDR-significant.

As shown in Fig. 5 (top), the elevated upper troposphere associated during summer with mode 1 extends to 20°N and the lower stratosphere although its zonally integrated values are only (locally) statistically significant near the tropopause north of 60°N, where the substantial elevation reaches the middle troposphere. The upper-tropospheric elevation varies geographically and is largest from northeastern Canada to Scandinavia although it is locally, but not FDR-significant at 250 hPa (Fig. 6a), unlike in the Arctic domain. Mode 1 is

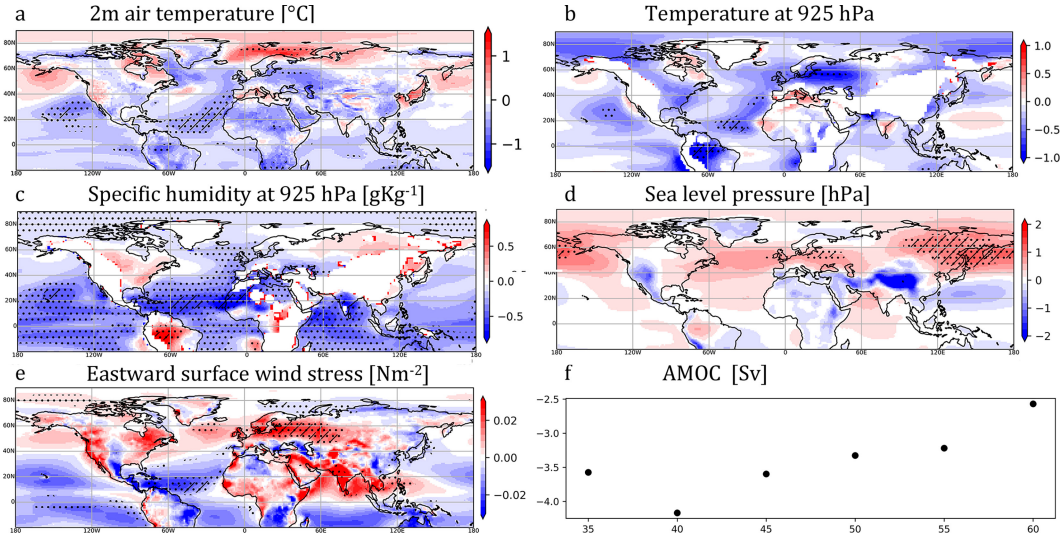

FIG. 8. Regression on SIC PC2 of various atmospheric variables (as indicated) during summer and the annual mean AMOC at several latitudes. Black dots (hatching) indicate elements that satisfy the FDR criterion north of 20°S at the 10% (5%) significance level.

related to warmer high-latitude SAT (Fig. 6b), albeit only FDR-significant over the Nordic seas and Barents Sea. The temperature signal is similar but smaller at 925 hPa (not shown), and the low-level specific humidity is generally higher than the MMM (Fig. 6c). Except above the Atlantic inflow into the Arctic and the warming hole region (Drijfhout et al. 2012), the summer SAT signal is mostly consistent with SST being driven by surface heat exchanges (e.g., downward heat flux over positive SAT; Fig. 6d), which are dominated in the extratropics by LW and SW radiation, while latent heat flux dominates in the tropics (not shown). The AMOC has no significant links to PC1 (not shown). Since there is no link with SLP, surface wind stress, or U850 in the extratropics, the main global links with mode 1 reflect near-surface thermodynamics. The regression patterns are similar with 14 models, but FDR significance is lost, suggesting that the global links with PC1 are rather weak (not shown).

b. *Links with SIC mode 2*

In the Arctic, the link between summer SAT and September SIC is closer for the dipolar mode 2 than for mode 1, with warm SAT preceding a negative SIC bias in the Atlantic sector and cold SAT, albeit near the coasts, preceding the positive SIC bias (Fig. 7b). However, the Atlantic sector warming does not extend to 925 hPa, and the lower troposphere is colder and, more significantly, dryer than the MMM in the broader Pacific sector (Figs. 7c,d). There is again a good correspondence between the SIC pattern and the net summer surface heat flux (Fig. 7e), which is dominated in the Pacific sector by SW radiation (Figs. 7f,g), consistent with larger summer SIC (Fig. 7n) and albedo, but moderated by upward LW radiation and turbulent heat fluxes over the incoming Atlantic waters (Figs. 7h–j), where the upward latent heat flux might reflect a response to the warmer SST. Interestingly, there is no link with downward LW radiation over the Arctic despite larger total cloud cover over sea ice (Fig. 7k). This differs from the links with mode 1, likely because larger cloud cover and lower specific humidity oppose in mode 2. Surface wind stress may also affect SIC mode 2 since there are significant links over much of the Arctic, with a larger southward component in the Greenland Sea and a southwestward component over the Barents Sea (Figs. 7o,p). No significant links are found in the troposphere and stratosphere (e.g., Fig. 5, bottom). In summary, September SIC mode 2 seems largely controlled by summer SW radiation fluxes and may involve ice drift. Warm and salty (Fig. 7l) incoming Atlantic waters likely contribute to the negative SIC bias in the Atlantic sector, again consistent with negative SIC in March (Fig. 7m), but the links with sea surface salinity are not FDR-significant. These links are less significant over the Arctic than for mode 1.

On the other hand, mode 2 has stronger global links with most variables, including FDR-significant tropical-wide signals. Except over the Nordic seas and Barents–Kara Seas, mode 2 is largely linked to cold summer SAT (Fig. 8a). The lower troposphere is colder (Fig. 8b) and, again more significantly, dryer (Fig. 8c) than the MMM, particularly over much of the ocean. Although there is no significant link with the zonally integrated geopotential height (Fig. 5, bottom) nor with Z250 (not shown), there are significant links with the lower troposphere, where SLP is largely positive between 40° and 70°N (Fig. 8d), significantly so over eastern Eurasia and the North Pacific, indicating a northward shift of the jet, with consistent U850 links (not shown). However, these features are not significant over the North Atlantic. In the tropics, the cold SSTs linked to mode 2 seem in part driven by strong trade winds (Fig. 8e), but the oceanic circulation may also contribute in the North Atlantic. Indeed, the SST has some limited analogy with a negative phase of the Atlantic multidecadal oscillation (AMO), and correspondingly, the AMOC is significantly weaker than the MMM at each latitude

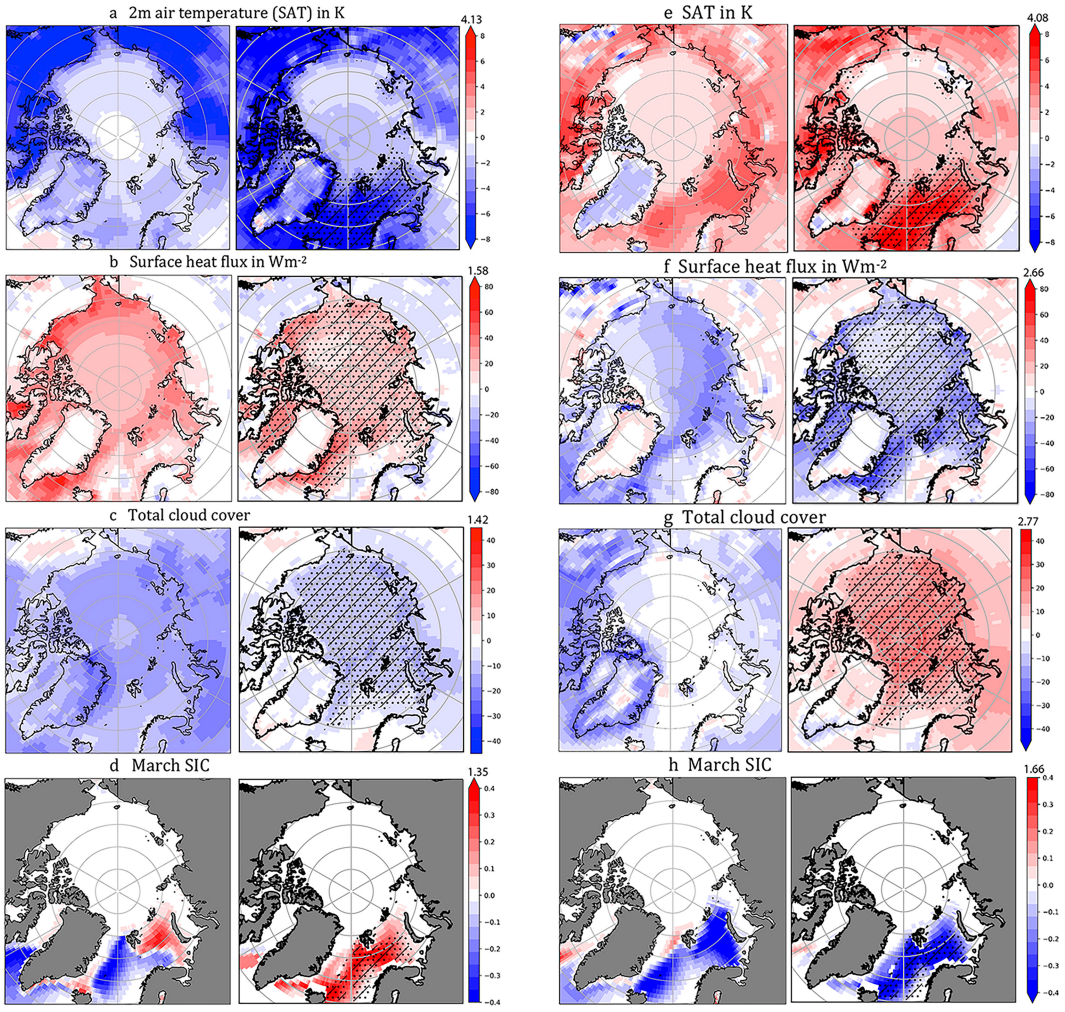

FIG. 9. (left) Departures from the MMM and (right) its reconstruction for various variables (as indicated) in NorCPM1 (left two panels) and IPSL-CM6-LR (right two panels). The lack of black dots (hatching) indicates that neither regression on the PCs was 10% (5%) FDR-significant. The multiplying factors of the reconstructed fields are indicated.

(Fig. 8f). Hence, the bipolar mode 2 seems significantly linked to both global atmospheric and oceanic circulations.

5. Reconstructing model variables from their links to SIC biases

For a variable Y_m in model m, regression (1) can be used to establish how much of its departure from the MMM is linearly linked to the two main modes of September SIC biases. This can be written as

$$Y_m^*(x) = a(x)\mathrm{PC1}(m) + b(x)\mathrm{PC2}(m), \tag{3}$$

where Y_m^* is the reconstructed deviation from the MMM. In the figures, grid points where a or b is significantly different from zero at the 10% level are indicated by dots. This may strongly overestimate significance if the two terms on the right-hand side of (3) have opposite signs, but the lack of dots correctly indicates that a reconstructed field is not significant at 10%. Since the analysis provides information on the relationships between summer means and September SIC biases, quantitative agreement with their reconstruction is not necessarily expected. More quantitative estimates would require integrating the sea ice equation, thus considering weighted atmospheric fields that would take into account their evolution and that of sea ice thickness and extent during summer and differences between SIC biases in late spring and early autumn instead of mean September SIC biases. This may be much noisier. Hence, for simplicity, we only focus on the similarity (or not) of the actual and reconstructed atmospheric patterns, and we scale the latter by a multiplicative factor to have the same spatial variance as the former. This was separately done for the Arctic and global domains, based on 60°–90°N and 20°S–90°N, respectively. The reconstruction of a few atmospheric and oceanic variables is next considered for the three models discussed earlier.

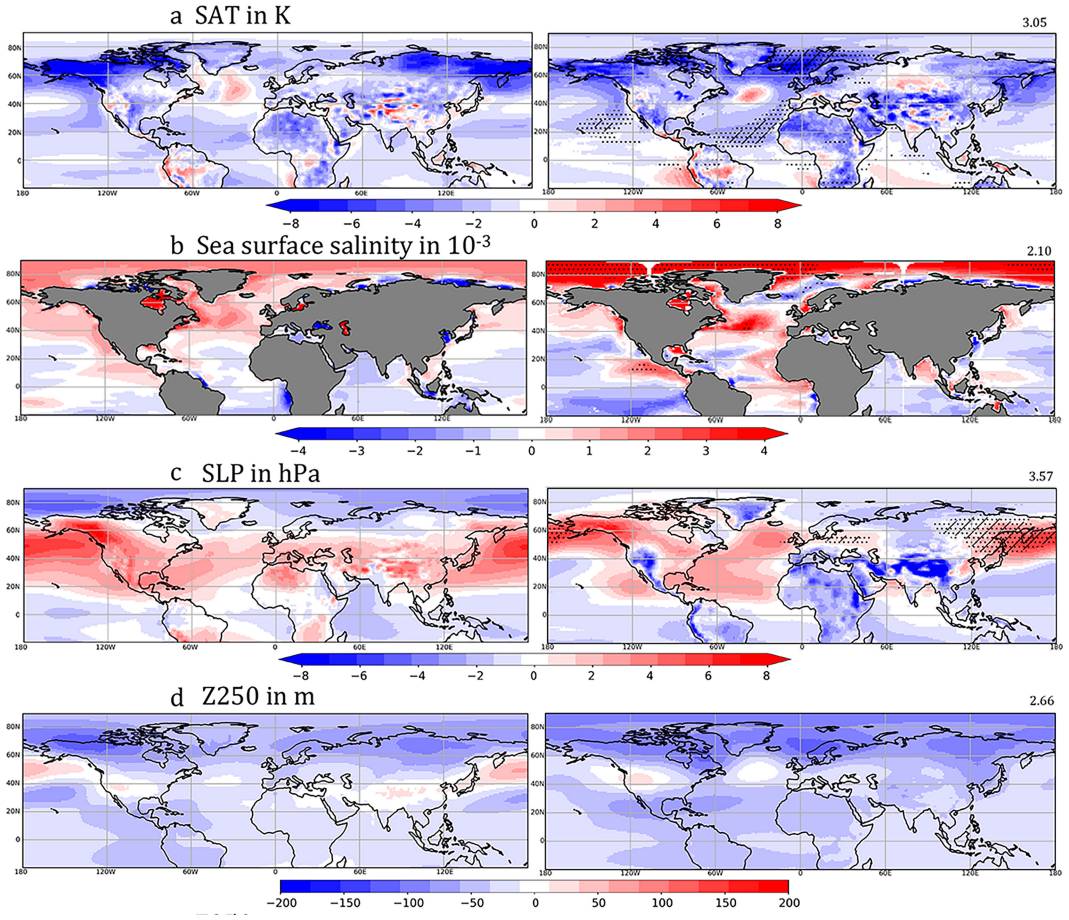

FIG. 10. (left) Departures from the MMM and (right) its reconstruction based on the two leading September SIC modes for various summer fields in NorCPM1, as indicated. The lack of black dots (hatching) indicates that neither regression on the PCs was 10% (5%) FDR-significant. The multiplying factors of the reconstructed fields are indicated.

a. NorCPM1

Recall that NorCPM1 has a positive SIC bias in September (Fig. 2) that projects negatively on SIC EOF1 and positively on EOF2 (Fig. 3). As shown in Fig. 9a, the reconstructed summer SAT shows good spatial correspondence with the negative SAT departure from the MMM in the Arctic domain, but the reconstructed cooling may be too strong in the Nordic seas and the Barents Sea, although the large multiplicative factor is affected by the mismatch over the continental areas. There are very good correspondences for the negative T925 and Q925 (not shown), as well as for surface heat flux (Fig. 9b), cloud cover (Fig. 9c), and summer SIC (not shown), but the correspondence is poor for surface wind stress (not shown). We argued in section 4 that both SIC modes were likely associated with a stronger Atlantic inflow. However, although PC1 and PC2 have opposite signs in NorCPM1, the negative PC1 dominates, suggesting somewhat weaker oceanic inflow, consistent with the negative reconstructed SSS (Fig. 10b) and SST in the Norwegian Sea, and large reconstructed March SIC (Fig. 9d). However, this does not agree with the departures from the MMM, where SSS is positive in the Norwegian Sea and March SIC only positive in the part of the Barents Sea. Lacking OHT data, one concludes that the oceanic influence on September SIC seems limited at best in NorCPM1.

On global scales, there is in most cases a surprisingly good pattern correspondence between the atmospheric departures from the MMM during summer and their reconstruction based on the two leading September SIC modes, albeit often with limited FDR significance. The (mostly negative) original and reconstructed SATs are largely similar (Fig. 10a), and so are T925 and Q925 (not shown). Cloud cover and the surface heat fluxes have more discrepancies although the correspondences are mostly good for the latent heat flux (not shown). Except in the Norwegian Sea, the tropical Atlantic, and the Bay of Bengal, the global SSS is rather well reproduced (Fig. 10b), and there is mostly good agreement for the surface wind stress (not shown). Despite little or no FDR significance, the pattern agreement for large-scale tropospheric variables is mostly good in the whole troposphere, as illustrated for SLP (Fig. 10c) and Z250 (Fig. 10d). This intriguing relation suggests that the biases of the September SIC in NorCPM1 might be closely linked to the global atmospheric circulation

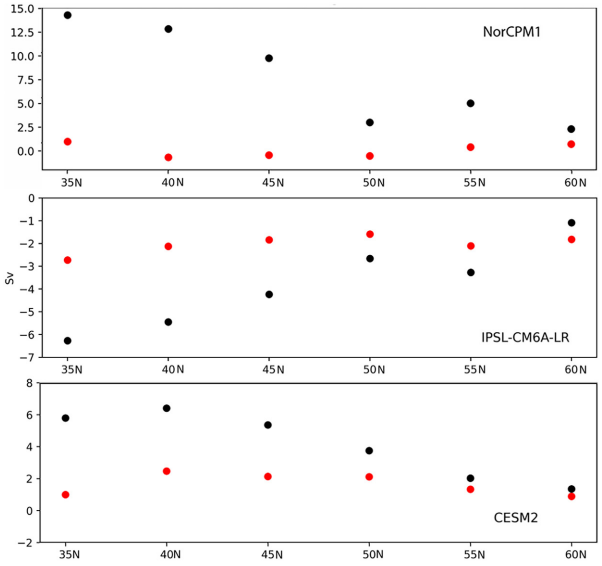

FIG. 11. Departure (Sv) from the AMOC MMM (black dots) and its reconstruction based on the two leading September SIC modes (red dots) for (top) NorCPM1, (middle) IPSL-CM6-LR, and (bottom) CESM2. No scaling was applied to the reconstructions. None of the reconstructed AMOC lacks significance, based on our criterion, since the links with PC2 were significant.

during summer, but larger sample sizes would be needed to resolve it.

The AMOC is very strong in NorCPM1 [32 Sv (1 Sv $\equiv$ 10^6 m^3 s^{-1}) at 40°N] and much larger than the MMM (Fig. 11, top, black dots). Yet the AMOC has negligible links with the two September SIC modes, as the reconstructed AMOC (red dots) is very small, consistent with the limited oceanic influence of the September SIC.

b. *IPSL-CM6-LR*

A different picture emerges for the IPSL-CM6-LR model, which projects positively on PC1 (i.e., negative September SIC bias) but only little on PC2 (Fig. 3). In the Arctic domain, the SAT (Fig. 9e) and the latent (not shown) and net (Fig. 9f) surface heat fluxes are well reconstructed even though the surface radiation fluxes are poorly reproduced, presumably due to the poor cloud cover agreement. Indeed, the reconstructed total cloud cover is positive (as expected from PC1), but the actual one is negative and very small over the Arctic Ocean (Fig. 9g). There is no agreement in the surface wind stress. By contrast, the SSS is very well reproduced in the Arctic, with mostly positive values in the Norwegian and Barents Seas (Fig. 12c), and March SIC is well reconstructed (Fig. 9h), suggesting larger Atlantic OHT into the Arctic. As IPSL-CM6-LR has the largest OHT across the Barents Sea Opening (Fig. 13) among the 12 models considered by Shu et al. (2022), this is consistent with a large OHT role in this model. Altogether, both the biases in local atmospheric air–sea heat exchanges and, in the Atlantic sector, stronger oceanic heat advection seem to influence September SIC bias in this model.

On the global scale, original and reconstructed SAT—mostly warmer north of 40°N and colder in the tropics (Fig. 12a)—and T925 (not shown) are well reproduced, suggesting significant global links with the SIC modes. To a lesser extent, surface heat flux (not shown), Q925—more humid above the extratropical oceans (Fig. 12b)—and SSS (Fig. 12c) also show good agreement. The AMOC departures from the MMM are negative, as expected from the weak AMOC in IPSL-CM6-LR (Boucher et al. 2020), and their reconstruction is qualitatively consistent at high latitudes (Fig. 11, middle). On the other hand, there is only limited agreement for surface wind stress (not shown) and little similarity for cloud cover (Fig. 12d), SLP, and U850 (not shown) and even opposite signs for Z250 (not shown). Hence, there are global links between low-level summer atmospheric thermodynamics and September SIC biases in IPSL-CM6-LR, but there is no link with the global atmospheric circulation.

c. *CESM2*

CESM2 has a negative SIC bias in September, which projects positively on PC1 and negatively on PC2 (Fig. 3). In the Arctic domain, the reconstructed summer SAT is broadly similar to the SAT departures from the MMM over sea ice, except that it is too warm over the Barents Sea and the Nordic seas, and often of opposite sign over the continents (Fig. 14a). The summer surface heat flux is mostly well reproduced, except in the Greenland Sea where the reconstructed flux is downward instead of upward (Fig. 14b) and in the northern subpolar gyre where it fails to reproduce the upward heat flux that is associated with warmer SST. The slightly higher SSS of the incoming Atlantic water is well reproduced (Fig. 14e), but in the Greenland Sea, SSS and SIC are poorly reproduced, as there is a small positive SIC bias in summer instead of a negative reconstructed one (not shown) and a larger one, albeit not FDR significant, in March (Fig. 14f), opposite to the large negative SIC in the reconstructions. This may be linked to discrepancies in both the surface heat flux and the meridional wind stress (not shown), which has negligible summer bias but is northward in the reconstruction due to SIC mode 2 (see Fig. 7p). Processes unrelated to the negative September SIC bias are thus at play in the Greenland Sea. The reconstructed March SIC also fails to reproduce the larger SIC in the eastern Barents Sea (Fig. 14f). This suggests that the Atlantic inflow penetrates less into the Barents Sea in CESM2 than in the MMM, which is consistent with a slightly lower OHT into the Barents Sea Opening than the 12-model average (Fig. 13). Interestingly, the positive Z250 departure from the MMM over the Arctic domain is reproduced (Fig. 14c). There is also good agreement for the larger cloud cover (Fig. 14d) and downward LW radiation (see Fig. 15c) over the Arctic Ocean.

On the global scale, the reconstructed SAT (Fig. 15a) and T925 (not shown) have similarities with their departures from the MMM, except over northern continents, but the match is poorer than for NorCPM1 and IPSL-CM6-LR. The summer surface heat fluxes (Fig. 15b) are better reproduced, with the heat flux seemingly responding to SST in much of the domain, away from the polar region. Interestingly, surface downward

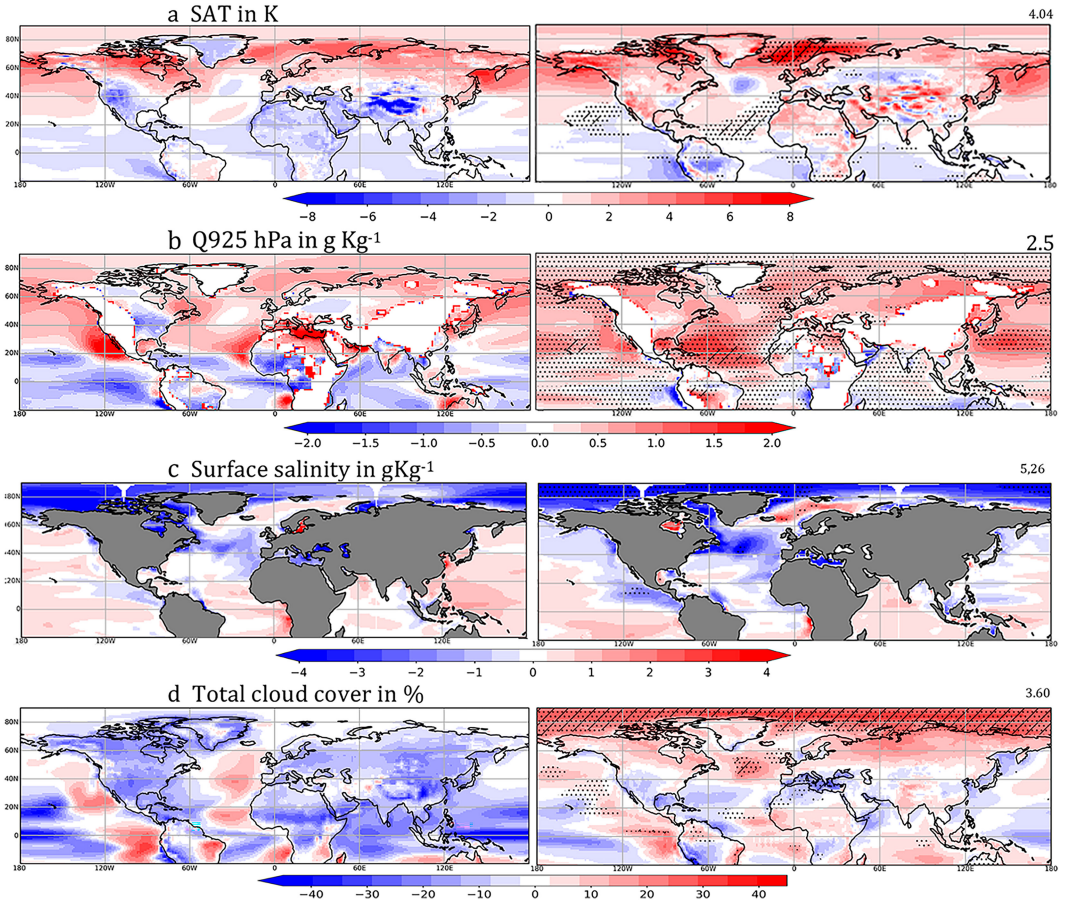

FIG. 12. As in Fig. 10, but for IPSL-CM6-LR.

LW radiation is larger than the MMM nearly everywhere and well reconstructed from the SIC modes (Fig. 15c), reflecting correspondingly well-reproduced excess of water vapor in the lower troposphere (Fig. 15d). On the other hand, there is little global correspondence between original and reconstructed fields for the lower tropospheric circulation (U850 and SLP) and none for surface wind stress and SSS (not shown). There is, however, some agreement for the (overestimated, see Danabasoglu et al. 2020) AMOC although the reconstructed positive AMOC is smaller (Fig. 11, bottom). In summary, the negative September SIC bias in CESM2 is linked to a few largely homogeneous global low-level atmospheric

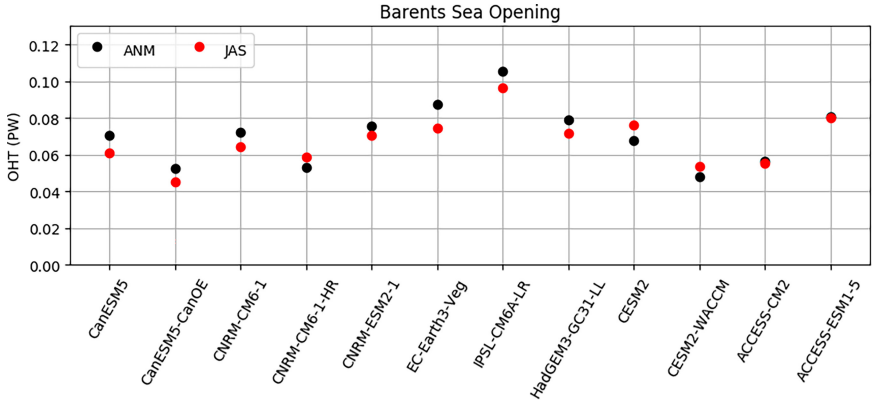

FIG. 13. Climatological mean OHT (PW) across the Barents Sea Opening for summer (red dots) and annual mean (black dots) for the 12 CMIP6 models considered by Shu et al. (2022).

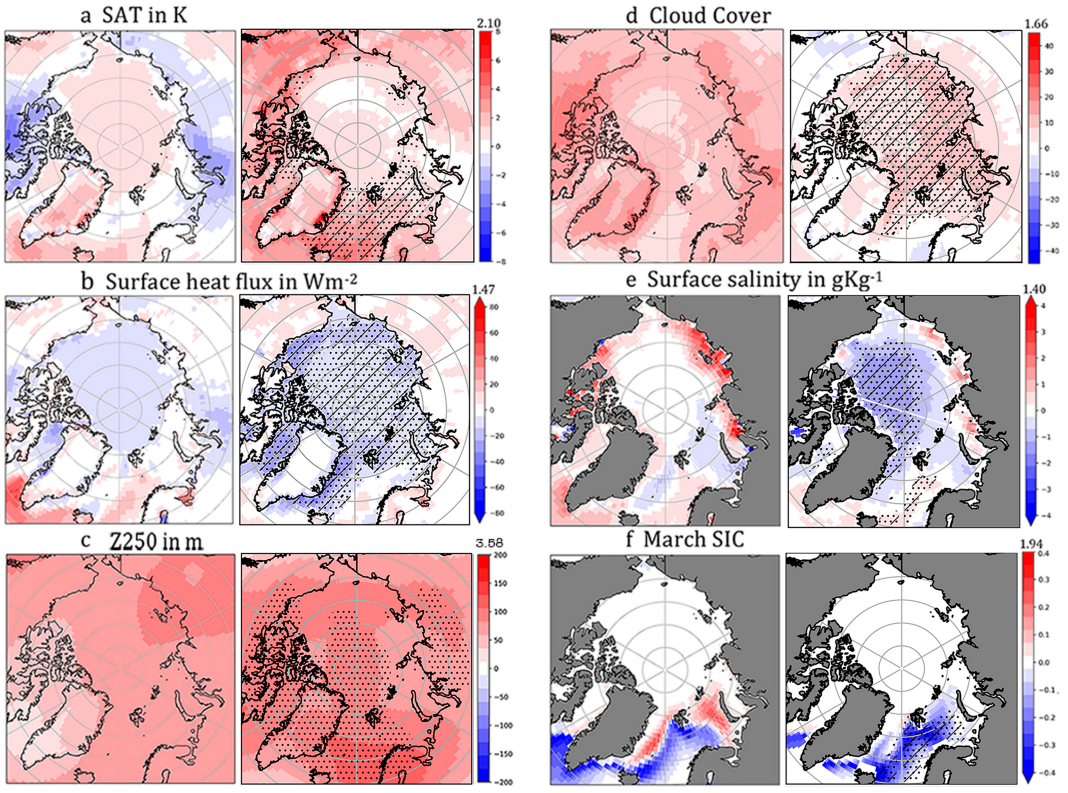

FIG. 14. As in Fig. 9, but for CESM2.

fields in summer that suggest a thermodynamic influence on SIC, without the obvious contribution of the Atlantic oceanic circulation.

6. Summary and discussion

The biases in the September SIC climatology simulated in historical simulations with 34 CMIP6 models were established, and the main patterns of intermodel SIC variability were estimated by EOF analysis. The first two EOFs represent 65% of the intermodel variance and provide a rather good representation of the September SIC biases. The linear relationship between the two SIC modes and the departures from the MMM of the climatology of atmospheric and a few oceanic variables were established by regression on the intermodel PCs. Atmospheric fields were considered in summer because of the limited sea ice persistence (Blanchard-Wrigglesworth et al. 2011) and its response time to atmospheric forcing. Although lagged correlations do not imply causality, we have tentatively interpreted them in this way when they are consistent with a plausible physical mechanism. Note that our statistical approach cannot address the discrepancy between MMMs and observations.

The first SIC mode, which accounts for half of the intermodel SIC variance, represents in its positive phase a smaller (than the MMM) SIC in the whole Arctic. In the Pacific sector, the negative SIC is mostly linked to larger summer downward LW radiation, consistent with larger total cloud cover and low-level specific humidity. However, in the Atlantic sector, SAT is significantly warmer, and the surface heat flux is dominated by smaller upward SW radiation consistent with reduced summer SIC, which affects the September SIC by the ice–albedo feedback. This seems in part linked to warmer and saltier incoming Atlantic Water, suggesting a larger OHT into the Arctic, which would be consistent with the smaller March SIC in the Barents Sea, a signature of large OHT (Zhang 2015; Årthun et al. 2019). Unfortunately, OHT estimates were only available for 12 of the 34 models, and there was much scatter in their relationship with the two SIC PCs. Furthermore, mode 1 exhibits no significant link to the AMOC although it was only available in depth coordinates. Mode 1 is also associated with a broad anticyclonic upper tropospheric high that exceeds 20 m above Greenland, northeastern Canada, and the North Atlantic sector of the Arctic. Since an upper-level anticyclone induces downward motion, adiabatic warming, and increased low-level cloudiness and relative humidity over the Arctic (e.g., Huang et al. 2021), this suggests that upper-level tropospheric circulation during summer may contribute to the negative SIC departure from MMM. The link is reminiscent of corresponding relationships discussed by Ding et al. (2017) for the observed SIC trends and their variability, which were supported by numerical experiments (see also Baxter and Ding 2022). They found that a stronger barotropic anticyclonic circulation in summer above Greenland and the Arctic Ocean increases the downwelling LW radiation above sea ice by warming and moistening the lower troposphere, reducing September SIC primarily in the Pacific sector. This is consistent

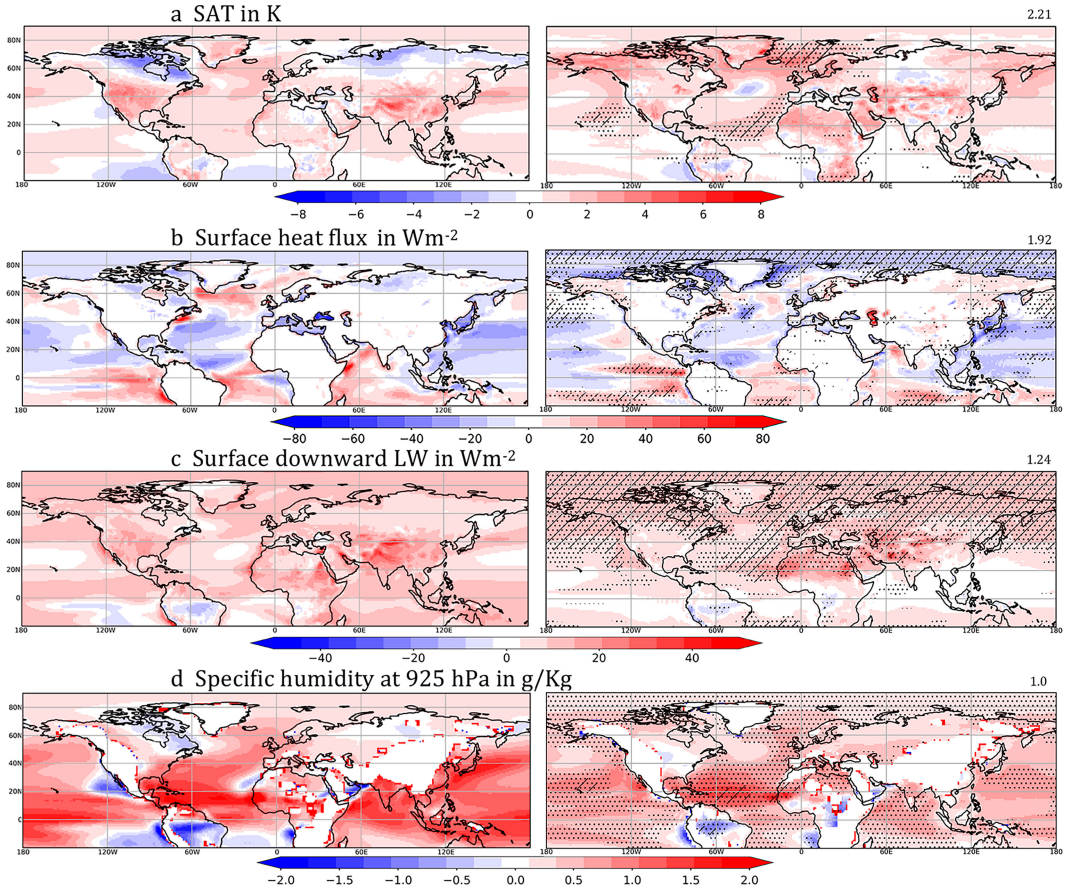

FIG. 15. As in Fig. 10, but for CESM2.

with our analysis since the SIC underestimation in the Atlantic sector may reflect larger OHT into the Arctic. In observations, Baxter et al. (2019) and Ding et al. (2019) found that the tropospheric perturbations and resulting sea ice loss seem influenced by tropical teleconnections driven by cold SST anomalies in the central tropical North Pacific. This SST pattern has no counterpart in the Pacific SAT bias associated with mode 1, but it may reflect that the links with remote SST forcing are weaker in CMIP6 models, as was the case for CMIP5 models (Baxter et al. 2019; Topal et al. 2020), or that the tropical SST influence on SIC may not be stationary (Bonan and Blanchard-Wrigglesworth 2020). In the extratropics, mode 1 is related to warmer extratropical summer surface and low-level tropospheric temperature and specific humidity. As it has little links with SLP and surface wind stress, its links with the atmospheric circulation are in very high latitudes and at upper levels. These relationships were broadly consistent with those based on the 14 models that had at least 8 ensemble members to reduce the influence of natural variability.

The second EOF of the intermodel variability of the September SIC climatology is a dipole that is positive in the Pacific sector and negative in the Atlantic sector, with corresponding summer SAT, but of opposite sign. However, the Atlantic sector warming does not reach 925 hPa. In the Arctic, mode 2 is closely linked to, hence seemingly driven by summer surface heat fluxes, with similar relations as for mode 1, except that there is practically no link with downward LW radiation. This likely occurs because the effects of larger cloud cover and lower specific humidity cancel out in mode 2. Mode 2 seems also related to warmer incoming Atlantic Waters, and unlike mode 1, it may be influenced by surface wind stress and ice drift. On global scales, mode 2 has strong and often significant global links. It is associated with mostly cold surface and lower-tropospheric temperature and negative specific humidity over the oceans. It lacks an upper-tropospheric link but is associated with a belt of high SLP that expands the high-pressure belt and shifts the jet northward, and to stronger trade winds that may explain the colder SST in the tropical Atlantic and Pacific. Oceanic circulation seems also linked to SIC mode 2 since the AMOC is weaker and there are some hints of a negative phase of the AMO. A weaker AMOC might seem at odds with warmer, saltier incoming Atlantic water, and high-latitude AMOC in density coordinates would be needed to investigate this further. In summary, bipolar mode 2 is linked to both global atmospheric and oceanic circulations, and the causes of its connection to the tropics would be worth investigating.

For each CMIP6 model, the relationships between the September SIC modes and departures from the MMM of the summer atmospheric and oceanic climatologies were used to reconstruct the latter, and the comparison was used to infer

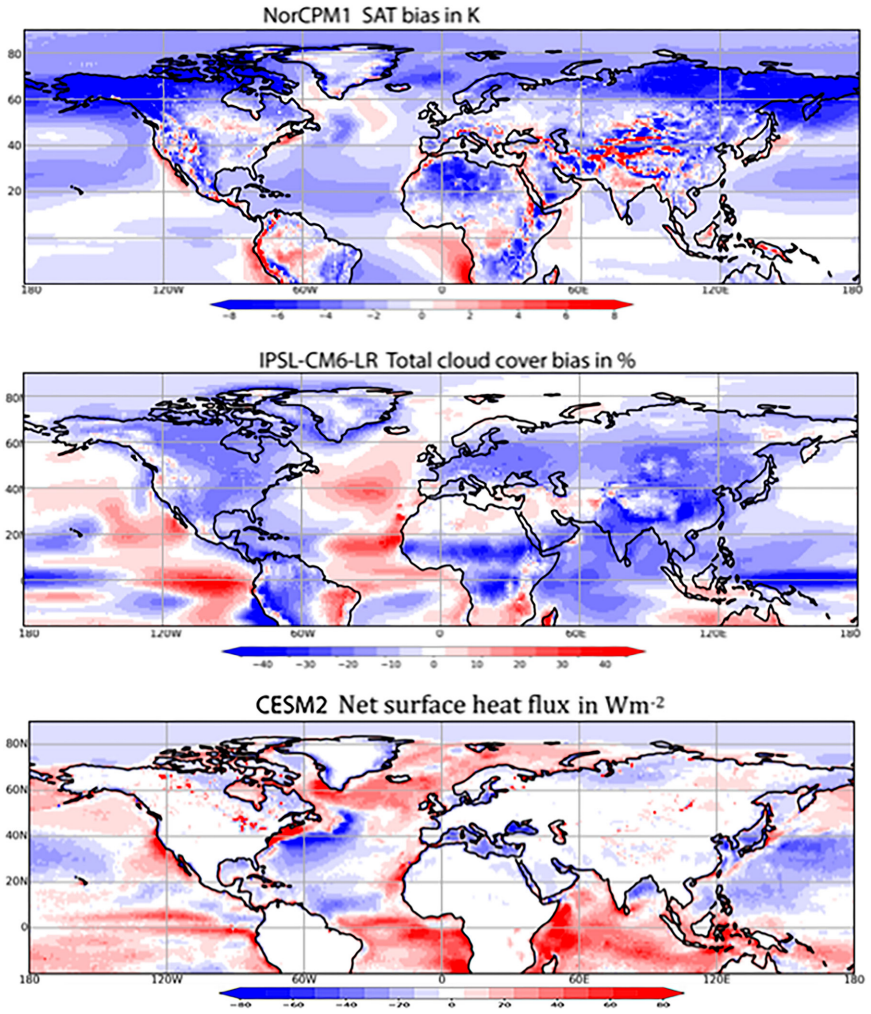

FIG. 16. Actual bias with respect to the ERA5 of SAT, total cloud cover, and surface heat flux in the three models, as indicated.

hints of their influence on September SIC bias. This was illustrated for three CMIP6 models that had at least 11 ensemble members: NorCPM1, which has too large September SIC, and IPSL-CM6-LR and CESM2, which have too small ones. Although our analysis only pertains to departures from the MMM, they are similar to the actual SIC biases (the differences from the observational estimates). This holds for the atmospheric variables, reflecting that the MMM biases of the 34 CMIP6 models are generally small. This is illustrated in Fig. 16, where the NorCPM1 SAT bias (Fig. 16a) compares well to Fig. 10a, the IPSL-CM6-LR total cloud bias (Fig. 16b) compares well to Fig. 11d, and the CESM2 net surface heat flux (Fig. 16c) compares well to Fig. 15b. Hence, the atmospheric reconstructions of the departures from the MMM can be considered a fair approximation of the model biases that are linked to September SIC biases. However, the resemblance with actual biases could not be verified for SSS and AMOC, which lack the required observational basis.

In the three models, the summer surface heat fluxes are mostly well reconstructed in the Arctic from the two September SIC modes, suggesting that they contribute to driving or sustaining the SIC biases. The comparison for Arctic SAT, Q925, and, to a lesser extent, T925 is generally good, while Arctic cloud cover is only well reproduced in NorCPM1 and CESM2 and opposite in IPSL-CM6-LR. The SAT, SSS, and March SIC provide indirect evidence of Atlantic inflow influence on SIC in the Atlantic sector, which seems stronger than the MMM in IPSL-CM6-LR and probably weaker in CESM2. The oceanic influence seems more complex in CESM2 since summer variables and March SIC are poorly reproduced in the Greenland Sea, and there is some evidence that Atlantic inflow penetrates less in the Barents Sea than predicted by the two SIC modes. Hence, processes unrelated to the negative September SIC bias are at play in the Atlantic sector. Consistent with our interpretation, IPSL-CM6-LR has the largest OHT across the Barents Sea Opening among the 12 models considered by Shu et al. (2022), while CESM2 has

a slightly weaker OHT than the average. For NorCPM1, OHT data were not available, and there is no evidence that the Atlantic oceanic circulation contributes to its large September SIC.

On global scales, the agreement with the reconstructions depends on the model and the variable considered, and caution is required as global FDR significance is often limited so that larger sample sizes would be needed to confirm the estimated relationships. In NorCPM1, the spatial agreement is remarkably good for summer SLP, U850, and Z250, suggesting that the September SIC biases are strongly linked to the global tropospheric circulation. There is no evidence of global oceanic circulation influence even though the AMOC is very strong in NorCPM1. A different picture emerges for IPSL-CM6-LR: the global links with the September SIC modes mostly reproduce well the low-level summer atmospheric biases (SAT, T925, and Q925) but not global cloud cover, SLP, U850, and Z250, suggesting no link with the global tropospheric circulation. However, the Atlantic oceanic circulation seems linked to the September SIC biases in the Atlantic sector since SSS and the weaker AMOC are reasonably well reproduced from the two SIC modes. In CESM2, the extratropical SAT is mostly warmer and surface heat flux weaker than the MMM, and they are rather well reproduced from the SIC modes. Interestingly, CESM2 has well-reconstructed, larger surface downward LW radiation and low-level specific humidity in most of the global domain. Otherwise, there is little correspondence between original and reconstructed tropospheric biases, and there is no obvious link with the Atlantic oceanic circulation. Hence, the negative September SIC bias in CESM2 seems mostly influenced by biases in global atmospheric thermodynamics.

In summary, Arctic September SIC bias is closely linked to biases in local atmospheric fluxes in summer, while the links with the Atlantic inflow and the global atmospheric circulations are model-dependent. Clear links to the North Atlantic oceanic circulation were only found in one of the three models that we discussed, namely, IPSL-CM6-LR. However, to better investigate the influence of the Atlantic oceanic circulation on September SIC, AMOC in density coordinates and additional oceanic variables should be considered, and OHT into the Arctic should be available for all the models. Similarly, investigating the links with biases in the September SIC trends during the historical period could provide further information on the drivers of the SIC biases. Finally, we note that our analysis was only applied to a limited number of CMIP6 climate models. Hence, more extended studies are needed.

Acknowledgments. L. Raillard was supported by a LOCEAN internship, and B. Ferster was supported by the ARCHANGE project of the "Make Our Planet Great Again" program (ANR-18-MPGA-0001, France). Support to C. Frankignoul and Y.-O. Kwon from NSF Grant 2106190 is gratefully acknowledged. We thank Q. Shu, F. Qia, and M. Årthun for generously providing the ocean heat transport data, G. Gastineau for his help with the FDR procedure, D. Oldenburg for useful discussions, and the three reviewers for their insightful and constructive comments that lead to a substantially improved manuscript. We acknowledge the World Climate Research Programme, which, through its Working Group on Coupled Modelling, coordinated and promoted CMIP6.

Data availability statement. The NSIDC sea ice concentration data are available at https://nsidc.org/data/G02202. The CMIP6 data are freely available from the CMIP6 ESGF node hosted by IPSL in France (https://esgf-node.ipsl.upmc.fr/projects/esgf-ipsl/).

REFERENCES

Årthun, M., T. Eldevik, and L. H. Smedsrud, 2019: The role of Atlantic heat transport in future Arctic winter sea ice loss. *J. Climate*, **32**, 3327–3341, https://doi.org/10.1175/JCLI-D-18-0750.1.

Baxter, I., and Q. Ding, 2022: An optimal atmospheric circulation mode in the Arctic favoring strong summertime sea ice melting and ice-albedo feedback. *J. Climate*, **35**, 6627–6645, https://doi.org/10.1175/JCLI-D-21-0679.1.

——, and Coauthors, 2019: How tropical Pacific surface cooling contributed to accelerated sea ice melt from 2007 to 2012 as ice is thinned by anthropogenic forcing. *J. Climate*, **32**, 8583–8602, https://doi.org/10.1175/JCLI-D-18-0783.1.

Bethke, I., and Coauthors, 2019: NCC NorCPM1 model output prepared for CMIP6 CMIP historical, version 3.3. Earth System Grid Federation, accessed 3 June 2022, https://doi.org/10.22033/ESGF/CMIP6.10894.

Blanchard-Wrigglesworth, E., K. C. Armour, C. M. Blitz, and E. DeWeaver, 2011: Persistence and inherent predictability of Arctic sea ice in a GCM ensemble and observations. *J. Climate*, **24**, 231–250, https://doi.org/10.1175/2010JCLI3775.1.

Bonan, D. B., and E. Blanchard-Wrigglesworth, 2020: Nonstationary teleconnections between the Pacific Ocean and Arctic sea ice. *Geophys. Res. Lett.*, **47**, e2019GL085666, https://doi.org/10.1029/2019GL085666.

Boucher, O., and Coauthors, 2020: Presentation and evaluation of the IPSL-CM6A-LR climate model. *J. Adv. Model. Earth Syst.*, **12**, e2019MS002010, https://doi.org/10.1029/2019MS002010.

Cox, C., T. Uttal, C. N. Long, M. D. Shupe, R. S. Stone, and S. Starkweather, 2016: The role of springtime clouds in determining autumn sea ice extent. *J. Climate*, **29**, 6581–6596, https://doi.org/10.1175/JCLI-D-16-0136.1.

Danabasoglu, G., and Coauthors, 2020: The Community Earth System Model version 2 (CESM2). *J. Adv. Model. Earth Syst.*, **12**, e2019MS001916, https://doi.org/10.1029/2019MS001916.

Ding, Q., and Coauthors, 2017: Influence of high-latitude atmospheric circulation changes on summertime Arctic sea ice. *Nat. Climate Change*, **7**, 289–295, https://doi.org/10.1038/nclimate3241.

——, and Coauthors, 2019: Fingerprints of internal drivers of Arctic sea ice loss in observations and model simulations. *Nat. Geosci.*, **12**, 28–33, https://doi.org/10.1038/s41561-018-0256-8.

Drijfhout, S., G. J. van Oldenborgh, and A. Cimatoribus, 2012: Is a decline of AMOC causing the warming hole above the North Atlantic in observed and modeled warming patterns?

J. Climate, **25**, 8373–8379, https://doi.org/10.1175/JCLI-D-12-00490.1.

England, M., A. Jahn, and L. Polvani, 2019: Nonuniform contribution of internal variability to recent Arctic sea ice loss. *J. Climate*, **32**, 4039–4053, https://doi.org/10.1175/JCLI-D-18-0864.1.

Hersbach, H., and Coauthors, 2020: The ERA5 global reanalysis. *Quart. J. Roy. Meteor. Soc.*, **146**, 1999–2049, https://doi.org/10.1002/qj.3803.

Huang, J., and Coauthors, 2017: Recently amplified Arctic warming has contributed to a continual global warming trend. *Nat. Climate Change*, **7**, 875–879, https://doi.org/10.1038/s41558-017-0009-5.

Huang, Y., Q. Ding, X. Dong, B. Xi, and I. Baxter, 2021: Summertime low clouds mediate the impact of the large-scale circulation on Arctic sea ice. *Commun. Earth Environ.*, **2**, 38, https://doi.org/10.1038/s43247-021-00114-w.

Jahn, A., J. E. Kay, M. M. Holland, and D. M. Hall, 2016: How predictable is the timing of a summer ice-free Arctic? *Geophys. Res. Lett.*, **43**, 9113–9120, https://doi.org/10.1002/2016GL070067.

Kapsch, M.-L., R. G. Graversen, M. Tjernström, and R. Bintanja, 2016: The effect of downwelling longwave and shortwave radiation on Arctic summer sea ice. *J. Climate*, **29**, 1143–1159, https://doi.org/10.1175/JCLI-D-15-0238.1.

Kay, J. E., M. M. Holland, and A. Jahn, 2011: Inter-annual to multi-decadal Arctic sea ice extent trends in a warming world. *Geophys. Res. Lett.*, **38**, L15708, https://doi.org/10.1029/2011GL048008.

Long, M., L. Zhang, S. Hu, and S. Qian, 2021: Multi-aspect assessment of CMIP6 models for Arctic sea ice simulations. *J. Climate*, **34**, 1515–1529, https://doi.org/10.1175/JCLI-D-20-0522.1.

Luo, R., Q. Ding, I. Baxter, X. Chen, Z. Wu, M. Bushuk, and H. Wang, 2023: Uncertain role in shaping summertime atmosphere-sea ice connections in reanalyses and CMIP6 models. *Climate Dyn.*, **61**, 1973–1994, https://doi.org/10.1007/s00382-023-06785-9.

Meier, W. N., F. Fetterer, A. K. Windnagel, and J. S. Stewart, 2021: NOAA/NSIDC climate data record of passive microwave sea ice concentration, version 4. National Snow and Ice Data Center, accessed 5 March 2022, https://doi.org/10.7265/efmz-2t65.

Mohino, E., B. Rodriguez-Fonseca, C. R. Mechoso, T. Losada, and I. Polo, 2019: Relationships among intermodel spread and biases in tropical Atlantic sea surface temperatures. *J. Climate*, **32**, 3615–3635, https://doi.org/10.1175/JCLI-D-18-0846.1.

North, G. R., T. L. Bell, R. F. Cahalan, and F. J. Moeng, 1982: Sampling errors in the estimation of empirical orthogonal functions. *Mon. Wea. Rev.*, **110**, 699–706, https://doi.org/10.1175/1520-0493(1982)110<0699:SEITEO>2.0.CO;2.

Notz, D., and Sea-Ice Model Intercomparison Project Community, 2020: Arctic sea ice in CMIP6. *Geophys. Res. Lett.*, **47**, e2019GL086749, https://doi.org/10.1029/2019GL086749.

Previdi, M., K. L. Smith, and L. M. Polvani, 2021: Arctic amplification of climate change: A review of underlying mechanisms. *Environ. Res. Lett.*, **16**, 093003, https://doi.org/10.1088/1748-9326/ac1c29.

Screen, J. A., and Coauthors, 2018: Consistency and discrepancy in the atmospheric response to Arctic sea-ice loss across climate models. *Nat. Geosci.*, **11**, 155–163, https://doi.org/10.1038/s41561-018-0059-y.

Serreze, M. C., A. P. Barrett, J. C. Stroeve, D. N. Kindig, and M. M. Holland, 2009: The emergence of surface-based Arctic amplification. *Cryosphere*, **3**, 11–19, https://doi.org/10.5194/tc-3-11-2009.

Shen, Z., A. Duan, D. Li, and J. Li, 2021: Assessment and ranking of climate models in Arctic sea ice cover simulations: From CMIP5 to CMIP6. *J. Climate*, **34**, 3609–3627, https://doi.org/10.1175/JCLI-D-20-0294.1.

Shu, Q., Q. Wang, M. Årthun, S. Wang, Z. Song, M. Zhang, and F. Qiao, 2022: Arctic Ocean amplification in a warming climate in CMIP6 models. *Sci. Adv.*, **8**, eabn9755, https://doi.org/10.1126/sciadv.abn9755.

Topal, D., Q. Ding, J. Mitchell, I. Baxter, M. Herein, T. Haszpra, R. Luo, and Q. Li, 2020: An internal atmospheric process determining summertime Arctic sea ice melting in the next three decades: Lessons learned from five large ensembles and multiple CMIP5 climate simulations. *J. Climate*, **33**, 7431–7454, https://doi.org/10.1175/JCLI-D-19-0803.1.

Wettstein, J. J., and C. Deser, 2014: Internal variability in projections of twenty-first-century Arctic sea ice loss: Role of the large-scale atmospheric circulation. *J. Climate*, **27**, 527–550, https://doi.org/10.1175/JCLI-D-12-00839.1.

Wilks, D. S., 2016: "The stippling shows statistically significant grid points": How research results are routinely overstated and overinterpreted, and what to do about it. *Bull. Amer. Meteor. Soc.*, **97**, 2263–2273, https://doi.org/10.1175/BAMS-D-15-00267.1.

Zhang, R., 2015: Mechanisms for low-frequency variability of summer Arctic sea ice extent. *Proc. Natl. Acad. Sci. USA*, **112**, 4570–4575, https://doi.org/10.1073/pnas.1422296112.